Atmospheric & Geodesic Controls on Muon Rate: A Numerical Study Based on CORSIKA

A. Cohu,[1] M. Tramontini,[2] A. Chevalier,[3] J.-C. Ianigro,[1] and J. Marteau[1]

[1]*Institut de Physique des 2 Infinis de Lyon (IP2I), IN2P3, CNRS, Université Lyon 1, UMR 5822, France*

[2]*CONICET, Facultad de Ciencias Astronómicas y Geofísicas, Universidad Nacional de La Plata, La Plata, Argentina*

[3]*MUODIM, 31 rue Saint-Maximin, 69003 Lyon, France*

Corresponding author: A. Cohu
Email address: a.cohu@ipnl.in2p3.fr

Abstract

Muon rate models play a key role in converting measured data into information on the density distributions of a target. Any given muography measurement, either in transmission or in scattering mode, requires a proper modelization of the muon flux according to the localization and to the atmospheric conditions. Two approaches are commonly used: either through semiempirical models calibrated on existing data or via Monte Carlo simulations. The former requires extrapolations to the field experiment conditions while the latter offers the advantage of tackling down, in a unique way, all relevant parameters such as barometric conditions, geomagnetic field, and atmosphere density. Although significant progress were made in the last decades, precision muography experiments require more and more accuracy on the models, especially for the muons close to the horizon where large disparities still remain. In this paper, we present detailed results obtained with the CORSIKA simulation framework to emphasize and quantify the impact of the environmental conditions on the sensitivity of muography measurements.

Keywords: CORSIKA, air shower, cosmic muon generator, muon tomography, atmosphere
DOI: 10.31526/JAIS.2022.250

1. INTRODUCTION

Applications of atmospheric cosmic rays (CRs) have grown in numbers in the last decade in the field of muography. Measurements of the muons flux attenuation or deviation have been successfully applied to the imaging or monitoring of large geophysical, archaeological, or industrial structures [1]. Among all charged particles reaching ground level, muons are the most numerous. Their energy loss or scattering when crossing a given length of the matter is exploited to reconstruct the material composition of the medium. The measurement of the muon energy is usually not possible in small and compact field detectors, which are standard trackers using particle physics techniques (scintillators, resistive plate chambers, micromegas, etc.). The simulation of the muon flux follows in general two different approaches:

(i) *Analytical models* which provide semiempirical formulas adjusted on experimental datasets; see, for example, Tang [2], Shukla [3], Honda [4], Gaisser [5], etc.

(ii) *Cosmic rays shower generators* which simulate extended air showers (EAS) from the primary cosmic rays down to the particles at the ground. The most popular are PARMA [6], CRY [7], MUPAGE [8], MCEq [9], CORSIKA [10], etc.

The sensitivity of the technique relies on the model's accuracy, which should take into account the experimental conditions in the most realistic possible way. For instance, it has been shown in Jourde et al. [11] and Tramontini et al. [12] that atmospheric conditions (pressure and temperature) are strongly correlated with the muon flux. It is also clear that the geomagnetic field may play a significant role by deflecting charged particles toward the poles [13], which leads to a decrease in the flux at the equator and an increase at high latitudes.

This article details the methodology of a flux simulation based on CORSIKA, a very flexible generator which allows changing the atmosphere and geomagnetic field profiles in a given place and time. We configured the hadronic interaction models and necessary options to obtain an accurate flux fitting our experimental data. We also show how the obtained model compares to various analytical models. We finally present numerical results on the effects of the geomagnetic field and atmospheric conditions (pressure, temperature, etc.) on the muon flux. A global conclusion is drawn on the obtained tool performance.

2. SIMULATION STRATEGY AND VALIDATION

2.1. CORSIKA's Parameters

CORSIKA (COsmic Ray SImulations for KAscade) is a Monte Carlo code for simulating atmospheric showers initiated by high energy cosmic ray. Primary particles (protons, light nuclei, etc.) are tracked in the atmosphere until they interact, decay, or are absorbed. All secondary particles are explicitly followed along their trajectories. Their parameters are stored when they reach an observational level. For more details on the physics involved in atmospheric showers processes, see reference [10]. In this study, we have selected CORSIKA's options that are believed to be essential to simulate the muon flux precisely and we detailed some of them below.

2.1.1. Hadronic Interaction Models and Primary Particles Trajectories

The primary CR flux is composed of several types of particles (H, He, C, O, Fe, etc.). When a primary particle reaches the top of the atmosphere, it undergoes hadronic interactions leading to the production of secondary CR. Among those particles, pions and kaons decay into muons. Different types of primary particle interaction models are available on CORSIKA. For the hadronic interaction models, we chose FLUKA for the low-energy interactions and QGSJET-II-4 for high energies, the best candidates in their energy domains.

The energy range of the primary particle is chosen to match the muon energy measurable in our tomography experiments: 10^1 to 10^7 GeV. This total range is split into several parts with a defined step. The number of simulated primary particles for a given energy range is weighted in each bin with an empiric law for the number of showers: $N = 10^{9-E}$ with $E = [1,7]$. This choice was also motivated by issues on computational time and systematic errors which increased considerably with the energy of the primary particle. The energy spectrum of primary CR follows a roughly exponential law: $E^{-\gamma}$. γ was calculated for each intermediate energy range with a fit defined by an analytical model describing the primary spectrum. We selected the Papini et al. model [14] based on real data fits. This reference allows us to take into account the solar modulation on the expected primary CR. The total flux was the sum of the fluxes of the various constituents of primary CR. It is possible to run simulations for each primary particle type or to apply the *superposition model* explained by Spurio [15] on the muon fluxes. We have chosen to use the last method. Then, the trajectories of particles are defined by their zenith and azimuth angles, ranging from 0° to 90° and from -180° to 180°, respectively. For zenith angles higher than 60°, the curvature of the atmosphere was taken into account since it cannot be neglected.

2.1.2. Earth's Magnetic Field

The Earth is protected by a magnetic shield created by the Earth's magnetosphere, which reduces the intensity of the high-energy flux reaching the ground. The geomagnetic field (B) modifies the spectrum of particles bombarding our atmosphere. This presents a low-energy cutoff, where the Earth's magnetic field is able to deflect primary CR below 10 GeV near the equator and close to 1 GeV at higher latitudes. The primary CR intensity also varies with longitude because of the asymmetry of the geomagnetic axis with respect to the Earth's rotation axis [17]. Those "East-West" fluxes show differences in energy intensity up to 100 GeV. This difference is more marked at high altitude than on the ground. Finally, there are significant local variations of the geomagnetic field, which affect the intensity of CR flux, the most famous being the South Atlantic Anomaly (SAA). All these effects can be taken into account in our simulation.

For each location, we declared the horizontal (B_x) and vertical (B_z) components of the Earth's magnetic field (in μT). They were generated by *NOAA geomagnetic calculator* according to reference [18]. CORSIKA computes the total magnetic field and its inclination from these two components. The main magnetic field effects were mostly latitude-dependent and therefore related to B_x, as we detail in Section 3.

2.1.3. Atmosphere Properties

The atmosphere can be divided into five layers: the troposphere, stratosphere, mesosphere, thermosphere, and ionosphere. The atmospheric profiles presented in Section 4 stop at the end of the stratosphere ($\sim$50 km). The troposphere is the part of the Earth's atmosphere located between the surface and an altitude of about 8 to 15 kilometers, depending on latitude and season. It is thicker at the equator than at the poles. This layer concentrates three-quarters of the atmospheric mass and the temperature decreases rapidly with altitude. The stratosphere extends, on average, between 12 and 50 km. It is characterized by an increase in temperature with altitude. The stratosphere begins at a low altitude near the poles, because the temperature is lower there. The distribution of atmospheric density is therefore different at high and low latitudes.

Muons are produced at a typical 10–15 km altitude (troposphere/stratosphere boundary). Their abundance is affected by the density differences in the atmosphere either by direct reinteraction or by modification of their parent mesons survival probabilities before decay [20, 21]. The effect is more important for high-energy muons, which result from high-energy mesons with larger lifetime due to time dilation and therefore with longer paths in the atmosphere. Thus, high-energy muons are more sensitive to temperature changes. An input to CORSIKA is therefore the atmosphere's state in which the CR ray showers are generated. The state of the atmosphere is described by the density of the air at each altitude level. This one was calculated by converting the relative humidity into saturation vapor pressure with the Magnus formula [19]. We computed the parameters and altitudes of the layer boundaries from ERA5 data, the latest climate reanalysis produced by the ECMWF which combines large amounts of meteorological observations with estimates made from advanced modeling and data assimilation systems. Some atmospheric density profiles are represented in Section 4.

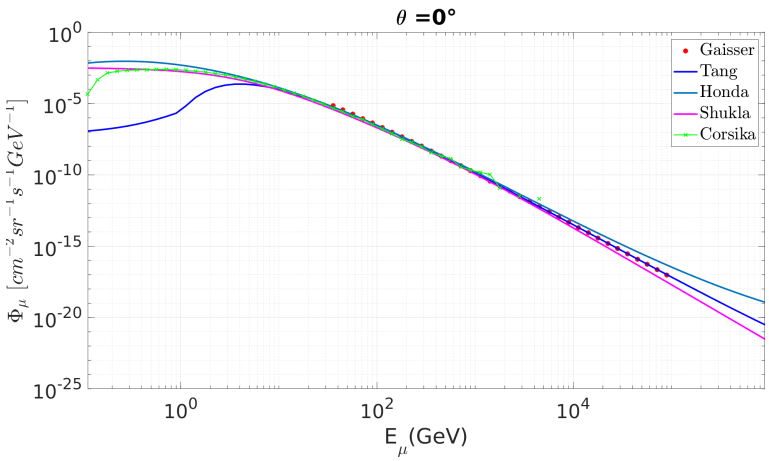

FIGURE 1: Differential fluxes as a function of muon energy for a given zenith angle $\theta = 0°$. Comparison between CORSIKA simulation and analytical models.

2.2. *Differential Fluxes from Analytical Models versus CORSIKA*

The fluxes simulated with CORSIKA according to the procedures, described before, were compared to analytical fluxes to check their relevance. For this purpose, we plotted differential fluxes as a function of muon energy only, for a muon zenith angle equal to 0°, in Figure 1. The simulated and the analytical fluxes did not agree with both at low and at high energies. Indeed, analytical models are known to be poorly adapted to small and large energies, because few measurements are available for their fitting equations. The CORSIKA model instead is probably more reliable over the whole energy range. Furthermore, analytical models are not extrapolated for all zenith angles, and they do not take into account geodesics parameters, a limitation overcome by the CORSIKA approach.

2.3. *Comparison of a CORSIKA Flux with Real Data*

The best validation cross-checks for any simulation is the comparison to real data. Data presented here were taken in Lyon (France, latitude 45° and close to sea level), in almost open sky conditions, with a 3-plane muon tracker (so-called muon telescope). We tilted the telescope progressively by step of 15° from the zenith ($\theta = 0°$) to the horizontal ($\theta = 90°$) directions. The muon flux is simulated in Lyon (France) respecting the geodesic constraints. Figure 2 displays the data/simulation comparison. Experimental points are the small crosses in blue, and the flux from CORSIKA's simulations is represented in black. A fit was made on the real dataset with a simple $\cos^2(\theta)$ at first order (in red). Despite the still pending disagreement at large zenith angles, we observed a real improvement in the data/model comparison with respect to the usual $\cos^2(\theta)$ (or analytical) fit, even though the simulation still underestimates slightly the data. To overcome this, it is necessary to constrain the simulated flux to the data to be as close as possible to reality.

3. NUMERICAL RESULTS: EFFECTS OF THE GEOMAGNETIC FIELD

In this section, we used our CORSIKA model, validated on a large dataset to simulate muon fluxes (E, θ) for various Earth magnetic fields. We wanted to quantify those effects on the measurable muon flux in the open sky. For this purpose, the atmospheric and altitude parameters have been fixed to constant values.

3.1. *Geomagnetic Field Model*

We decomposed the geomagnetic field along B_x and B_z components as described in Section 2.1.2.

To test the B_z influence, we fixed a horizontal component and we varied vertical components. Only a slight difference at high zenith angles was observed. The B_z component did not seem to play a significant role in the muon flux. We also control this by varying separately the horizontal and vertical components for a fixed total field B.

To understand the B_x influence, we have set the vertical component at the constant value $B_z = 20\,\mu$T, and we performed two simulations, respectively, with $B_x = 15\,\mu$T and $B_x = 45\,\mu$T. We computed the ratio of those two configurations for four different energy ranges (1–10, 10–100, 100–1000, and 10^3–10^4 in GeV) and for different zenith angles.

3.2. *B_x Influence Results*

Figure 3(top), on the left panel, presents the normalized intensity distribution of the flux ratio over the zenith angle, for each individual energy range. It shows that when considering a higher energy range, the intensity ratios distribution (1–10^4 GeV) tends to a narrow peak centered at 0.95 ± 0.04, the median value, corresponding to a small effect of about 5%. As expected, the ratio tends

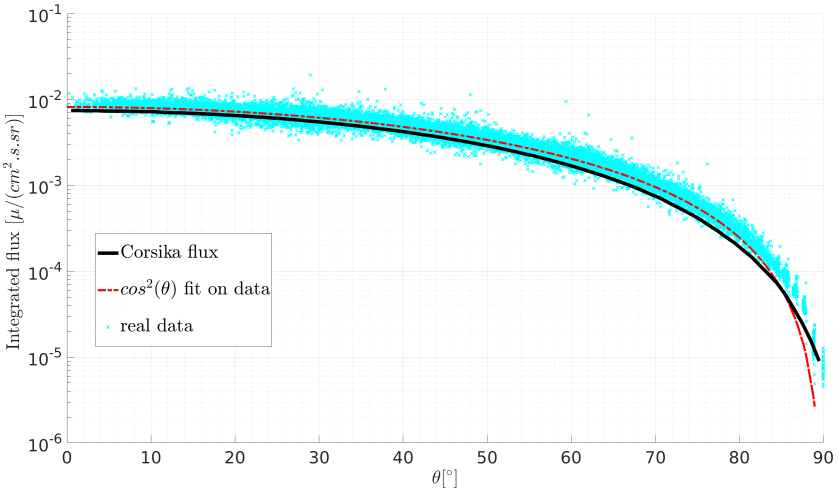

FIGURE 2: Integrated muon fluxes plotted as a function of the zenith angle θ. The crosses represent the measured data for different inclinations of the detector. The red line is a linear fit in $\cos^2(\theta)$ on the total measured flux. The black line represents the simulated flux with CORSIKA.

to one for energy ranges greater than 10 GeV but affects the low-energy particles which are more deflected toward the poles. Right panel shows the flux ratio with respect to the zenith angle θ for fixed energy ranges.

At low energies (1 to 10 GeV in dark blue), the flux is higher for $B_x = 45\,\mu$T until 60° and between 85° and 90° and lower between 60 and 85°. This probably arises from the fact that high-angle particles have to cross a larger section of the atmosphere and therefore may start their travel with higher energies, making them less sensitive to the geomagnetic field's effect. Note that this sample dominates over the total integrated flux ratio (in black) which follows more or less the same behavior.

As expected, at high energies, typically above 10 GeV, the flux ratio remains more constant with the zenith angle (in light blue, green and orange). Note that this high-energy sample is usually not used in scattering mode. Therefore, one has to pick corrections for the geomagnetic effects to perform absolute measurement with scattering muography.

All the results presented in this section are subject to significant uncertainty, which is dominated by statistical errors (systematic errors not shown). Those errors increase with the particles, energy since much less high-energy and large-angles muons were simulated due to limits imposed essentially by computational time.

4. NUMERICAL RESULTS: ATMOSPHERIC PARAMETERS, INFLUENCE

We wanted to quantify the impact of atmospheric density on the flux, which is ultimately controlled by the temperature and the pressure of the atmosphere. Hence, at the same location, seasonal variations affect the muon flux over time. For our tests, we chose the city of Lyon in France (lat = 45.75, long = 4.75, $B_x = 22.71\,\mu$T, $B_z = 40.96\,\mu$T), where we performed the open sky measurements shown in Figure 2. The atmosphere density parameters used to simulate muon fluxes with CORSIKA are determined with "era5tool" and ERA5 datasets, for two different dates.

4.1. Atmosphere Models

Temperature and density profiles in Lyon, during winter (12/30/20) and summer (08/01/19), are displayed in Figure 4. These temperature and density profiles highlight which part of the atmosphere may affect the muon flux production and filtering. We observe that the density of the atmosphere globally decreases with altitude and that colder atmospheres are denser, especially at lower altitudes. Note that around 10-15 km there is a temperature inversion (Figure 4(top)) which is relevant since this is the typical altitudes where muons are generated after their parents, decay.

4.2. Atmosphere Flux Comparison: Seasonal Effects

Figure 5 presents the normalized intensity distribution for different energy ranges: 1–10 GeV, 10–100 GeV, 100–10^3 GeV, and 10^3–10^4 GeV and the distribution for the whole energy range. It shows that when considering a larger energy range, the intensity distribution tends to a narrow peak centered at 0.92 ± 0.01, the median value, which means that the flux is 10% higher in winter in Lyon (France). This effect is quite sizeable and must be properly accounted for when precise muography is required over for low-opacity targets. This effect depends of course on the particles, energy. The right panel shows the flux ratio for different zenith angles θ in the range 0 to 90° when considering the same energy ranges. It shows that in summer the flux is higher for high energies (100 to 10^4 GeV, in green and orange) and lower in winter. For lower energies, the flux ratio is higher in winter (1 to 100 GeV, in

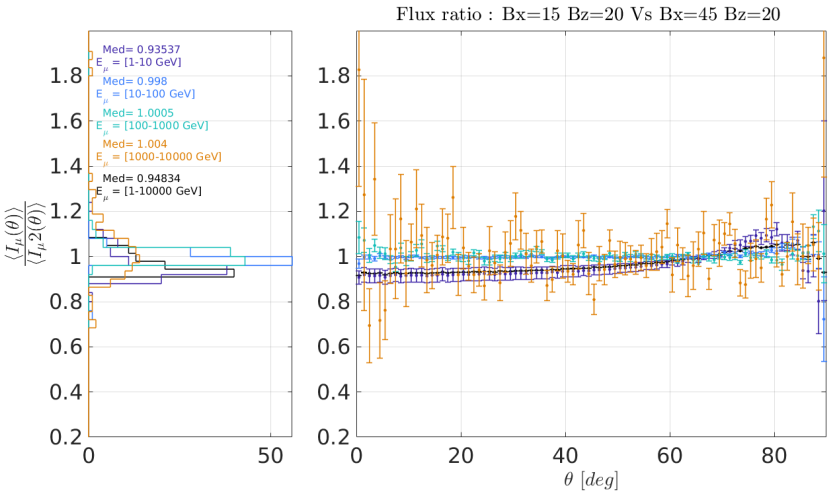

FIGURE 3: (Left) Normalized intensity distribution for different energy ranges from 1 to 10^4 GeV (in color) and for the whole energy range (in black). (Right) Flux ratio dependence on the zenith angle θ between two different magnetic field fluxes for the same energy ranges. Statistical errors are plotted for 1σ. The different magnetic parameters are (1) $B_x = 15\,\mu$T, $B_z = 20\,\mu$T and (2) $B_x = 45\,\mu$T, $B_z = 20\,\mu$T with same atmospheric conditions and altitude.

light and dark blue) and lower in summer. These effects increase with the zenith angles θ. Statistical errors of fluxes simulations are present in Figure 5 as in Section 3 and fixed to 1σ. They prevailed over systematic errors and were not considered.

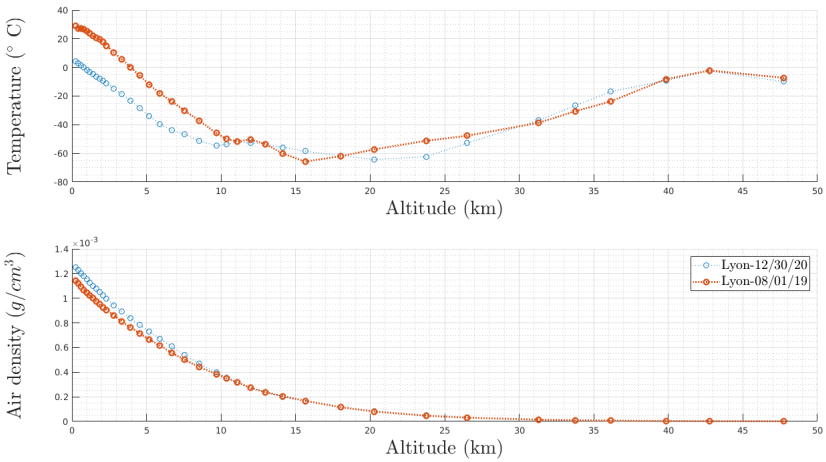

FIGURE 4: Temperature (top) and density (bottom) profiles for altitudes from 0 to 50 km in Lyon during winter (30/12/20) in blue and in summer (08/01/19) in red.

The decrease in atmospheric density should increase the muon flux. We have seen before that the effect is more important for high-energy muons, which result from high-energy mesons with larger lifetime due to time dilation and therefore with longer paths in the atmosphere. We observed this effect in Figure 5 where the flux increases by 1% during summer. Given the associated error bars, nothing can be concluded. However, the low-energy muons are more important in winter. There is therefore another process than the absorption of low-energy muons in the atmosphere, e.g., the temperature inversion observed around 10–15 km altitude in Figure 4. Indeed, at this altitude, the temperature affects particularly the mesons and may account for the significant 8% effect which is observed in Figure 5.

5. CONCLUSION

In this paper, we presented a muon flux simulation workflow accounting for muon-atmosphere interactions, based on the CORSIKA framework. We detailed our simulation strategy and the various relevant inputs from the hadronic interaction models to the atmosphere conditions. In particular, we used meteorological ERA5 pressure and temperature datasets to compute the required at-

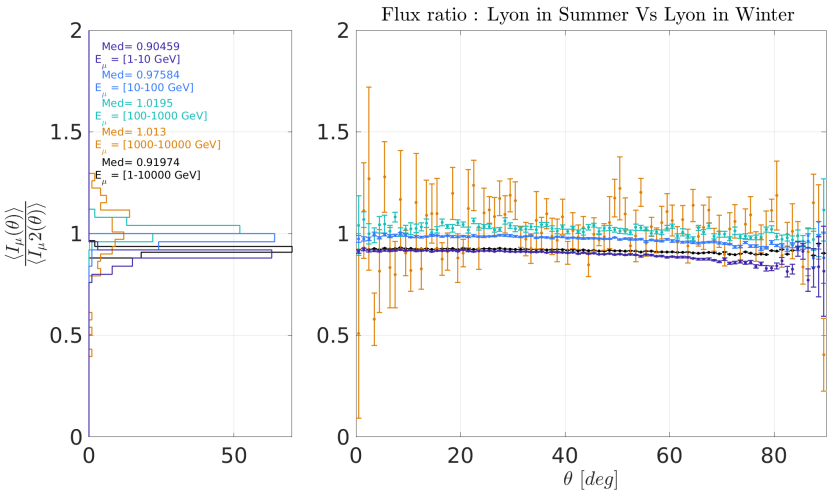

FIGURE 5: (Left) Normalized intensity distribution for several energies ranging from 1 to 10 000 GeV (in color) and for the whole energy range (in black). (Right) Flux ratio as a function of the zenith angle θ in summer and winter conditions in Lyon, France, for the same energy ranges. Statistical errors are plotted for 1σ. The different atmosphere conditions were (1) 08/01/2019 and (2) 12/30/20, with constant geomagnetic field and altitude.

mospheric density profiles. The workflow has been cross-validated against experimental data and standard semiempirical models found in the literature. Simulations prove themselves to be a powerful tool to study and make predictions on effects induced by the geomagnetic field or the atmospheric seasonal variations. Those effects are of increasing importance when one wants to produce muon imagery and/or long-term monitoring, on both ends of the opacity spectrum. Low-opacity target imagery is controlled by low-energy muons filtered out by the density of the atmosphere. On the other side, high opacity target imagery is largely affected by the process at stake for high-energy muon production. In particular, those effects may affect significantly muon scattering experiments using mostly low-energy muons. This study opens the gate to develop semiempirical formulas predicting the evolution of the muon energy spectrum for each zenith angle, in relation to the atmospheric state. These formulas will be useful to correct recorded muon fluxes on the fly, when direct open-sky measurements are not available or not sufficiently refined in terms of energy description.

CONFLICTS OF INTEREST

The authors declare that there are no conflicts of interest regarding the publication of this paper.

ACKNOWLEDGMENTS

This work was the subject of a CIFRE agreement between the ArcelorMittal Maizières Research SA and IP2I (Lyon).

References

[1] J. Marteau et al., Journal of Instrumentation **12.02: C02008** (2017).
[2] A. Tang et al., Phys. Rev. **D74(5)**, 053007 (2006).
[3] P. Shukla, S. Sankrith, Phys. Rev. **A33(30)**, 1850175 (2018).
[4] M. Honda et al., Phys. Rev. **D75(4)**, 043006 (2007).
[5] T. K. Gaisser, Cambridge, UK: Univ (1990).
[6] T. Sato, PloS one, **10(12)**, e0144679 (2015).
[7] C. Hagmann et al., IEEE Nuclear Science Symposium Conference Record (Vol. 2, pp. 1143–1146) (2007).
[8] G. Carminati et al., Computer Physics Communications, **179(12)**, 915–923 (2008).
[9] A. Fedynitch et al., In The 34th International Cosmic Ray Conference (Vol. 236, p. 1129) (2016).
[10] D. Heck et al., Report fzka, **6019(11)**, (1998).
[11] K. Jourde et al., Scientific reports, **6(1)**, 1–11 (2016).
[12] M. Tramontini et al., Earth and Space Science, **6(10)**, 1865–1876 (2019).
[13] J. Clay, In Proceedings of the royal academy of sciences amsterdam (Vol. 31, pp. 1091–1097) (1928).
[14] P. Papini et al., Il Nuovo Cimento **C19(3)**, 367–387 (1996).
[15] M. Spurio, Springer, In Particles and Astrophysics, pp. 23–54 (2015).
[16] D. Heck, Forschungszentrum Karlsruhe (2004).
[17] S. Pethuraj, arXiv preprint arXiv:1905.00739 (2019).
[18] A. Tapia et al. (2016).

[19] P. Abreu, Astroparticle Physics, **35(9)**, 591–607 (2012).
[20] T. K. Gaisser et al., Cosmic rays and particle physics, Cambridge University Press (2016).
[21] E. W. Grashorn et al., Astroparticle Physics, **33(3)**, 140–145 (2010).